Journal of
Materials Chemistry B

Materials for biology and medicine

Accepted Manuscript

This article can be cited before page numbers have been issued, to do this please use: J. H. Kim, B. Hui, J. Lee, K. Lee, J. Kim, Y. Kim, M. H. Chua, J. Xu, M. G. Lee, X. Liu and J. S. Kim, *J. Mater. Chem. B*, 2025, DOI: 10.1039/D5TB01253H.

ROYAL SOCIETY OF CHEMISTRY

rsc.li/materials-b

View Article Online
DOI: 10.1039/D5TB01253H

PET-leveraged ALDH probe toward cancer stem cells

Ji Hyeon Kim,[a,‡] Bryan Yat Kit Hui,[b,c,‡] Jieun Lee,[a,‡] Kyeong-woo Lee,[a] Jungryun Kim,[a] Yujin Kim,[a] Ming Hui Chua,[c] Jianwei Xu,[c, d] Min-Goo Lee,[a,*] Xiaogang Liu,[b,*] Jong Seung Kim[a,*]

[a] Department of Chemistry, Korea University, Seoul 02841, Korea.

[b] Science, Math and Technology Cluster, Singapore University of Technology and Design (SUTD), 8 Somapah Road, Singapore 487372, Singapore.

[c] Institute of Sustainability for Chemicals, Energy and Environment (ISCE2), Agency for Science, Technology and Research (A*STAR), 1 Pesek Road, Jurong Island, Singapore 627833, Singapore.

[d] Department of Chemistry, National University of Singapore (NUS), 3 Science Drive 3, Singapore 117543, Singapore.

‡ These authors contributed to this work equally.

Abstract

Developing novel aldehyde dehydrogenase (ALDH) probes is essential for enhancing the localization and visualization of cancer stem cells (CSCs) by improving specificity and signal-to-noise ratios. This study introduces four new ALDH fluorescent probes (**AldeCou 1–4**), designed using a coumarin-linker-benzaldehyde scaffold. Among them, **AldeCou-1** exhibits a significant stokes shift of 125 nm ($\lambda_{ex}/\lambda_{em}$ = 380/505 nm), which enhances the signal-to-noise ratio and minimizes inner-filter effects. **AldeCou-1** demonstrated superior green fluorescence imaging in A549 and MDA-MB-231 cells, enabling differentiation between these cell lines based on ALDH activity. Compared to conventional ALDH activity assay kits, such as ALDEFLUOR, which require additional buffers and inhibitors that complicate imaging protocols, **AldeCou-1** enables simplified assay conditions by eliminating the need for ATP-binding cassette (ABC) transporter inhibitors and specialized buffers. Computational analysis suggests that the fluorescence turn-on mechanism of **AldeCou-1** is driven by ALDH-mediated photoinduced electron transfer (PET). These findings provide valuable mechanistic insights and pave the way for developing next-generation ALDH probes for improved CSC screening and characterization.

View Article Online
DOI: 10.1039/D5TB01253H

KEYWORDS: Cancer stem cells; ALDH; Fluorescent Probes; Photoinduced Electron Transfer

Introduction

Cancer stem cells (CSCs) are cells with stem cell characteristics within tumors, and they remain an obstacle to cancer treatment[1-6] by causing tumor progression and heterogeneity due to their ability for self-regeneration and differentiation.[2, 7] The high drug efflux system and quiescent cell cycles make CSCs chemo-resistant, limiting the effectiveness of chemotherapy. This might lead to recurrence and metastasis, as CSCs can regulate the gene expression of epithelial-to-mesenchymal transition (EMT).[8-11, 12, 13] On the other hand, aldehyde dehydrogenase (ALDH) is an enzyme that catalyzes the oxidation of aldehydes to carboxylic acids through $NAD(P)^+$-dependent oxidation.[14] Recent investigations support that ALDH is a widely recognized CSC biomarker in most cancer types. An overexpression of ALDH in CSCs increases the metabolism of toxic aldehydes into carboxylic acids, which lowers oxidative stress in CSCs and promotes cancer cell survival.[15] Therefore, developing fluorescence probes to detect high ALDH activity levels ($ALDH^{High}$) in cells is a valuable strategy for assessing and locating the populations of CSCs.[16-18]

Using fluorescent probes to detect ALDH enzymes is a promising strategy due to fast response times and non-invasive and non-destructive detection, enabling live cell imaging and analysis. ALDH fluorescent probes usually consist of an aldehyde group, which is oxidized into carboxylic acids by intracellular ALDH enzymes.[19, 20] The low lipophilicity of the oxidized carboxylic acids groups restricts the permeability of these oxidized probes across biological membranes.[21, 22] The retention of these probes within the cell leads to the accumulation of oxidized ALDH fluorescent probes in CSCs which enables high sensitivity and specificity during the fluorescence imaging of CSCs.[23] In other words, the current design of ALDH probes leverages on this oxidative response towards intracellular ALDH enzymes and the hydrophobic nature of the resulting oxidized carboxylic acid groups to become effective CSC markers.[17, 18, 24, 25] The fluorescence turn-on response mechanism of ALDH probes has been discussed by other groups, where they attribute this response to either photoinduced electron transfter (PET) or intramolecular charge transfer (ICT) mechanisms. Li, Tang, and Duan, developed a fluorene–thiophene oligomer-based probe that exhibits an excellent 365-fold fluorescence intensity enhancement when detecting ALDH1A1, an isoform of ALDH. They attributed the turn-on fluorescence response to the suppressed ICT following

View Article Online
DOI: 10.1039/D5TB01253H

the oxidation of the aldehyde sensor to the carboxylate.[18] Anorma *et al.* had designed a rhodamine-based ALDH probe that exhibits a ~20-fold fluorescence turn-on response *via* a donor-photoinduced electron transfer (d-PET) mechanism when sensing ALDH1A1.[25] Chan's group further developed a red fluorescence emitting ALDH probe based on a xanthene scaffold that also use PET as a fluorescence turn-on mechanism.[26] As one of the most widely recognized ALDH probes, ALDEFLUOR is often utilized in flow cytometry analysis to compare and sort CSC populations based the ALDH activity.[19, 27] However, CSCs not only overexpress ALDH, but exhibit elevated levels of ATP-binding cassette (ABC) transporters, such as MDR1, MRP2, and BCRP.[28] As ALDEFLUOR is also a substrate for ABC transporters, ALDEFLUOR assays require additional buffers containing ABC transporter inhibitors for flow cytometry analysis, which poses challenges when imaging is needed in a natural cell medium. As such, the development of next-generation ALDH fluorescent probes must be unaffected by the effluxion mediated by ABC transporters. This improvement would enhance detection accuracy, increase the signal-to-noise ratio, and eliminate the need for additional buffer solutions during flow cytometry.[29]

In this study, we have designed four novel ALDH fluorescent probes, **AldeCou 1-4**, based on a coumarin-linker-benzaldehyde scaffold. Unlike other reported fluorescent turn-on ALDH probes, which have a fully conjugated structure to facilitate efficient electron/charge transfer mechanisms,[16, 18, 25, 26, 30] we incorportated linker groups bearing an sp^3 alkyl-secondary amine scaffold that disrupts conjugation between the fluorophore and the ALDH substrate. Although Yagishita *et al.* had previously reported the incorporation of a flexible alkyl linker into their design with a rhodamine-linker-benzaldehyde scaffold, the poor stokes shift of 22 nm potentially hinders the quantum efficiency of their probes.[23] Instead, **AldeCou-1** not only has characteristics of conventional ALDH probes (accumulation within $ALDH^{high}$ cells and a fluorescence turn-on response), but it also exhibits a significant stokes shift of 125 nm ($\lambda_{ex}/\lambda_{em}$=380/505 nm) which is one of the largest stokes shift amongst ALDH probes to date, which greatly reduces self-absorption and improved signal-to-noise ratio.[31] Moreover, we observed that our probes are not expelled from CSCs; in other words, our probes can perform live cell imaging and flow cytometry analysis without specific buffers. These experimental findings suggest that our probes can be more conveniently used in ALDH activity detection assays than conventional kits. An additional new finding of our AldeCou series was that ALDH isoform selectivity is influenced by the linker length in the chemical

View Article Online
DOI: 10.1039/D5TB01253H

structure. For example, AldeCou-1, which contains a shorter linker, was reactive toward both ALDH1A1 and ALDH3A1, whereas AldeCou-2, with a longer linker, was reactive toward ALDH1A1 but not ALDH3A1. This characteristic was reflected in fluorescence imaging, which revealed a marked difference between AldeCou-1 and AldeCou-2 in HeLa cells that endogenously overexpress ALDH3A1. Furthermore, our computational studies considers the conformational dynamics of our probes arising from the flexible linkers, and we unravel a through-space PET mechanism instead of the conventional intramolecular PET. This rationalization of through-space PET in our study not only explains the fluorescence turn-on response of our probes, but also paves the way for future ALDH probes with more advanced designs and to explore different fluorescent turn-on mechanisms. As such, these experimental and computational findings provide insight and considerations into future designs of high-performance ALDH fluorescent probes.

Materials and Methods

All the materials used for the synthesis were purchased from Aldrich (St. Louis, MO, USA), TCI (Tokyo, Japan), Alfa-Aesar (MA, USA), and SYinnovation (Kyeongi, Korea) and used without further purification. ALDH1A1, and ALDH3A1 were purchased from NKMAX (Kyeongi, Korea). TLC Silica gel 60 F254, 0.25 mm (Merck) and PLC Silica gel 60 F254, 1 mm (Merck) were used for analytical and preparative thin layer chromatography. ^{1}H and ^{13}C NMR spectra were collected in NMR solvents ($CDCl_3$, MeOD) on a Brucker 500 MHz spectrometer (MA, USA). The mass spectra were obtained using an LC/MS-2020 Series (Shimadzu) and Compact Q-TOF (Bruker) from Sogang University. The reaction mixtures were prepared by combining ALDH enzyme, 100 mM KCl, 2 mM DTT, and 1 mM NAD^+ (for ALDH1A1) or 1 mM $NADP^+$ (for ALDH3A1) in 100 mM pH 7.5 Tris buffer solution with 1% DMSO.

General synthesis protocol of the intermediates, probes AldeCou-1-4, AcidCou-1 and characterization. The four probes comprise of a common coumarin fluorophore, varying 1,2,3-triazole-alkyl-amine linkers across the four probes, and a common 4-methyl benzaldehyde substrate. The synthetic routes are outlined in ESI Schemes S1 and S2, and detailed procedures for the synthesis of intermediates and final compounds are provided in ESI Section 1.1. A brief description of the synthesis of the probes **AldeCou1-3** follows the preparation of the alkyl

View Article Online
DOI: 10.1039/D5TB01253H

linkers functionalized with azides (**1**, **7**, and **12**) through past reported procedures, with the size of the alkyl linker varies from propyl, hexyl, and propyl for **AldeCou-1**, **AldeCou-2**, **AldeCou-3**, respectively. Compounds **1**, **7**, and **12** then react with a protected benzaldehyde moiety (2 and 3) *via* S_N2 to generate the benzaldehyde-alkyl linker fragments (**4**, **8**, and **13**). Next, a common alkyne functionalized coumarin fragment, **5**, reacts with **4**, **8**, and **13** *via* azide-alkyne Huisgen cycloaddition to generate the precursors **6**, **9**, and **14**. Lastly, the precursors **6**, **9**, and **14** were reacted with 4 M HCl for acid-catalyzed hydrolysis of the acetal group into the benzaldehyde fragments to generate **AldeCou-1**, **AldeCou-2**, and **AldeCou-3**, respectively. On the other hand, **AldeCou-4** was prepared *via* the nitrile reduction of 4-(bromomethyl)benzonitrile to **15**, followed by the conversion into the azide **16** before Huisgen cycloaddition with **5** to form the **AldeCou-4**. (See Scheme S1 and Scheme S2 for the detailed synthetic pathways) All intermediates and final compounds were characterized by ^{1}H NMR, ^{13}C NMR, and ESI-MS, with the characterization data provided in the Supporting Information (ESI Section 2, Figures S1-42).

Spectroscopic Characterization. UV-Vis spectra were recorded on a Jasco V-750 spectrometer (Tokyo, Japan), and FL spectra were recorded on a Jasco FP-8500 spectrofluorometer (Kyoto, Japan). Analytical or preparative high-performance liquid chromatography (HPLC) was performed on a ReproSil 100 C18 (5 μm, 4.6 x 250 mm) column using ChroZen (YL-Clarity). EPR measurements were conducted by JES-X320 (MA, USA) at Kangwon National University. Stock solutions of **AldeCou-1, AldeCou-2, AldeCou-3, AldeCou-4,** and **AcidCou-1** were prepared in DMSO with 10 mM concentrations and diluted into 10 μM.

Reverse Phase HPLC Analysis. Analysis was performed to investigate the conversion of **AldeCou-1** into **AcidCou-1**. The reaction was initiated by adding ALDH1A1 (3.33 μg/mL) and NAD^+ (1 mM) to the **AldeCou-1** (10 μM) solution. Aqueous 100 mM Tris pH 7.5, 100 mM KCl, and 2 mM DTT with 1% DMSO as a co-solvent was used for all solution test experiments. The mixture was then incubated at 37 °C for sufficient time to allow complete conversion into carboxylate. To monitor the conversion of aldehyde to carboxylate, each sample was eluted at a flow rate of 1 mL/min using the mobile phase (solvents A: deionized water containing 0.1% TFA and solvent B: acetonitrile) with a binary gradient (Solvent A: 60% for 5 min, 60% to 20% for next 15 min, 20% to 0% for 1 min, 0% for 10 min).

Selectivity Testing of Physiological Analytes. 10 mM of fluorescence probe (**AldeCou-1**, **AldeCou-2**, **AldeCou-3**, and **AldeCou-4**) was diluted into 10μM in Tris-buffer (100 mM, pH 7.5) containing 100 mM KCl and 1%

View Article Online
DOI: 10.1039/D5TB01253H

DMSO. Then, an oxidant (H_2O_2), a reductant (GSH), metal salts ($ZnCl_2$, $CaCl_2$, $MgCl_2$, and CuSO4), and amino acids (Cysteine, Glucose, and Serine) were added to the mixture solution respectively. ALDH1A1 (3.33 μg/mL), NAD^+ (1 mM), and DTT (2 mM) were added to the mixture solution. The concentration was as follows: H_2O_2 (2 mM), GSH (100 μM), $ZnCl_2$ (100 μM), $CaCl_2$ (2 mM), $MgCl_2$ (2 mM), $CuSO_4$ (50 μM), Cysteine (1 mM), Glucose (10 mM), and Serine (1 mM). All reactions were incubated at 37 °C for 1 hour and excited at 390 nm.

Cell Lines and Reagents. Human breast cancer cell line MDA-MB-231 was purchased from Korea Cell Line Bank (Seoul, Korea). MDA-MB-231 was cultured in RPMI 1640 media (HyClone, Chicago, IL, USA). All media were supplemented with 10% FBS (GIBCO, Grand Island, NY, USA) and 1% penicillin/streptomycin (GIBCO), and cells were cultured at 37 ℃ in a humidified atmosphere with 5% CO_2.

Cellular Imaging. MDA-MB-231 cells and A549 cells (5.0×10^4 per dish) were plated in 35-mm confocal glass bottom dishes and allowed to adhere for 24 h. For living cell imaging following N,N-diethylaminobenzaldehyde (DEAB) treatment, DMSO or 1 mM of DEAB (diluted from 100 mM DEAB) was pretreated for 1 h. Subsequently, the cells were treated with **AldeCou-1** and **AldeCou-2** (diluted from 10 mM DMSO stock solution). After 2 h incubation, the cells were washed twice with PBS, and the fluorescence emission was recorded. For $ALDH^{High}$ or $ALDH^{Low}$ MDA-MB-231 cells (5.0×10^4 per dish) were seeded in 35-mm confocal glass bottom dishes (SPL) and incubated for 24 h. Then, 20 μM of **AldeCou-1** and **AldeCou-2** in the media was treated. After 30 min incubation, the cells were washed twice with media and incubated for the next 2 h before the fluorescence emission was recorded. Confocal laser scanning microscope (CLSM) images were obtained using an Olympus FV3000 confocal laser scanning microscope with *ex/em* wavelength set at 405/505 nm. Fluorescence intensity was measured by image J program.

Flow Cytometry

ALDH Activity Assays of AldeCou Probes. Assays were performed in PBS containing 2% FBS. 5×10^5 MDA-MB-231 cells were incubated with 10 μM **AldeCou** series at 37 °C for 30 min. For DEAB control, 1 mM DEAB was incubated with 10 μM **AldeCou** series. Cells were centrifuged for 5 min at 250 × g, and the supernatant was removed, exchanged to fresh 2% FBS in PBS buffer, and kept on the ice. FACSymphony A1 Cell Analyser (BD

View Article Online
DOI: 10.1039/D5TB01253H

Bioscience) was used for detection. **AldeCou** series were detected by the BV480 channel (ex/em 405/480 nm), and voltages were tuned to detection.

AldeCou-1 ALDH Activity Assays with ABC Transporter Inhibitors. Assays were performed in PBS containing 2% FBS. 5×10^5 MDA-MB-231 cells were incubated with DMSO (null), MK571 (50 μM), Verapamil (20 μM), or Novobiocin (200 μM) with 10 μM **AldeCou-1** or ALDEFLOUR at 37 °C for 30 min. Cells were examined using the same procedure described above. **AldeCou-1** was detected by the BV480 channel, ALDEFLOUR was detected by the FITC channel (ex/em 488/515 nm), and voltages were tuned to detection.

ALDEFLOUR Assay and Cell Sorting. According to the manufacturer's instructions, the ALDEFLUOR™ Kit was used for ALDH Assays (StemCell Technologies, Durham, NC, USA). Briefly, after harvesting MDA-MB-231 cells, they were washed with PBS and resuspended in ALDEFLUOR assay buffer containing the ALDEFLUOR reagent at 2.5 x 10^5 cells per assay. The cells were then incubated for 30 min at 37°C. As a negative control, a fraction of the cells were treated with 15 μM diethylaminobenzaldehyde (DEAB), a specific inhibitor of ALDH. The DEAB-treated cells were used to baseline the fluorescence intensity of the negative control population. The ALDH-positive and ALDH-negative cell populations were analyzed using a BD Accuri™ C6 Plus flow cytometer (BD Biosciences, San Jose, CA, USA) and FlowJo™ v10.8 Software (BD Life Sciences). The ALDEFLUOR substrate was excited at 488 nm, and emission was detected in the FL1 channel. To isolate the $ALDH^{high}$ and $ALDH^{low}$ subpopulations, sorted cells were collected using a FACSAria flow cytometer (BD Biosciences). The same gating strategy described above confirmed the purity of sorted populations. After sorting $ALDH^{high}$ and $ALDH^{low}$ cells through cell sorter, cells were stabilitzed by subculturing for 4 days before conducting confocal imaging or flow cytometry. To separate sub-populations enriched in $CD133^+$ and $CD133^-$ cells, the magnetic-activated cell sorting (MACS) was conducted following the procedure reported in a previous report.[32]

Computational Methodology. Ground state conformational analysis, geometry optimizations, and electronic energy calculations in ground states were conducted using density functional theory (DFT). Excited state energies and geometry optimizations were conducted using time-dependent density functional theory (TD-DFT). Both DFT and TD-DFT calculations were performed in Gaussian 16 software.[33-35] DFT calculations were performed using ωB97XD and M06-2X functionals to cross-check the results.[36-38] Most TD-DFT calculations of the excited states were performed using M06-2X and 6-31+g(d,p) basis set unless stated otherwise.[39, 40] Solvation effects were

View Article Online
DOI: 10.1039/D5TB01253H

considered by deploying the SMD solvent model and corrected linear-response (cLR) approach in H_2O.[41-43] The optimized molecular geometries in the locally excited (LE) and electron transfer (ET) excited states were confirmed through frequency analysis of vibrational modes. Avogadro software was used to visualize the optimized geometries and molecular orbitals of the compounds.[44] During the optimization of the adiabatic electron-transfer state of **AldeCou-1**, TD-DFT calculations using the M06-2X/6-31+g(d,p) level of theory were unsuccessful. We then attempted a hybrid approach of optimizing the excited state geometries using B3LYP/6-31+g(d,p), followed by single point energy correction using m062x/6-31+g(d,p). However, this treatment is still unsuccessful for **AldeCou-2, AldeCou-3**, and **AldeCou-4**. As such, we report the successful computational results for **AldeCou-1**. While using the M06-2X and B3LYP functional, we employed GB3 empirical dispersion correction to account for intramolecular interactions.

Results and Discussion

Optical properties, substrate selectivity, and flow cytometry analysis of AldeCou-1-4. The structures of the four coumarin-based ALDH fluorescent probes are shown in Figure 1A. λ_{abs} of the four probes ranges from 380 to 395 nm, while the four probes all showed a common maximum emission λ_{em} at 505 nm, with varying intensities (Figure S44A and B), suggesting that the size of the linker had little effect on the spectral peaks of the four probes. We first tested the fluorescence properties of the four probes with ALDH1A1 in aqueous Tris-buffer solution at physiological pH with NAD^+ as an oxidant. After 15 minutes of incubation, the probes showed a two-to-three-fold increment in fluorescence intensities, reaching *ca.* 1000 – 1300 emission arbitrary units (a.u.) except for AldeCou-3 which did not exhibit strong emission (*ca.* 400 a.u). AldeCou-1 and AldeCou-2 appeared to reach their maximum emission intensity after 30 and 25 minutes, respectively, of *ca.* 1300 a.u, corresponding to a three-to-four-fold increment in their emission intensities (Figure 1B). We also tested the fluorescence turn-on selectivity of our probes towards ALDH1A1 against other common physiological analytes such as various metal ions (Zn^{2+}, Ca^{2+}, Mg^{2+}, and Cu^{2+}), hydrogen peroxide (H_2O_2), glutathione, amino acids (Cys and Ser), and glucose. All four probes show a clear selectivity towards ALDH1A1 with NAD^+, as represented by a two-to-five-fold emission intensity difference compared to the other analytes (Figure S45). We additionally evalulated the stability of AldeCou-1 in the presence of oxidants such as H_2O_2, potassium superoxide (KO_2), and tert-Butyl hydroperoxide (t-BuOOH) by measuring absorbance and fluorescene spectra of various 0.1 mM and 1 mM solutions of these oxidants incubated

View Article Online
DOI: 10.1039/D5TB01253H

with AldeCou-1 (Figure S46). The negligible spectral changes after 30 minutes of incubation suggest that AldeCou-1 is sufficiently stable and do not undergo unwanted oxidation by other oxidants.

Motivated by the turn-on characteristic of the probes towards ALDH1A1, flow cytometry analysis was conducted in A549 cells. To ascertain if the increase in emission intensities is indeed in response to ALDH, we gated cells that showed a fluorescence enhancement by comparing them to cells treated with DEAB, an ALDH inhibitor. A549 cells treated with **AldeCou-3** and **AldeCou-4** showed a much lower percentage of stained cells (0.99 and 12.8 %, respectively) than those treated with **AldeCou-1** and **AldeCou-2** (61.5 and 38.4 %, respectively; Figure 1C). Next, we monitored the change in fluorescence intensity over 30 min for **AldeCou-1** and **AldeCou-2** with ALDH1A1 and ALDH3A1 (Figure 1D), two overexpressed ALDH enzymes in cancer and CSCs.[45] **AldeCou-1** showed a similar oxidative response towards both ALDH1A1 and ALDH3A1, where a similar emission of *ca.* 1200 units was reached after 20 min. However, **AldeCou-2** showed higher selectivity towards ALDH1A1 than ALDH3A1, where the fluorescence intensity of **AldeCou-2** with ALDH3A1 is approximately half that with ALDH1A1. This could be one explanation for **AldeCou-1** exhibiting a larger population of stained cells compared to **AldeCou-2** (61.5 versus 38.4 %, respectively) (Figure 1C). To evaluate the differential activity of **AldeCou-1** and **AldeCou-2** toward ALDH1A1 and ALDH3A1, we compared the fluorescence imaging of both probes in HeLa cells, since HeLa cells exhibit significantly higher expression of ALDH3A1 compared to A549 and MDA-MB-231 cells, and ALDH3A1 levels were markedly greater than those of ALDH1A1 (Figure S47A). Given that **AldeCou-2** is selective toward ALDH1A1, it exhibited only weak staining in HeLa cells, in contrast to **AldeCou-1**, which yielded a much stronger signal. This result underscores the functional difference between **AldeCou-1** and **AldeCou-2** in cells with distinct ALDH isoform profiles, indicating that ALDH3A1 activity can be reflected in live-cell fluorescence imaging. In light of the fact that both ALDH1A1 and ALDH3A1 are linked to cancer stemness, **AldeCou-1** is more suitable for detecting cancer stem cells. Thus, we selected it for subsequent cellular imaging and computational studies.

View Article Online
DOI: 10.1039/D5TB01253H

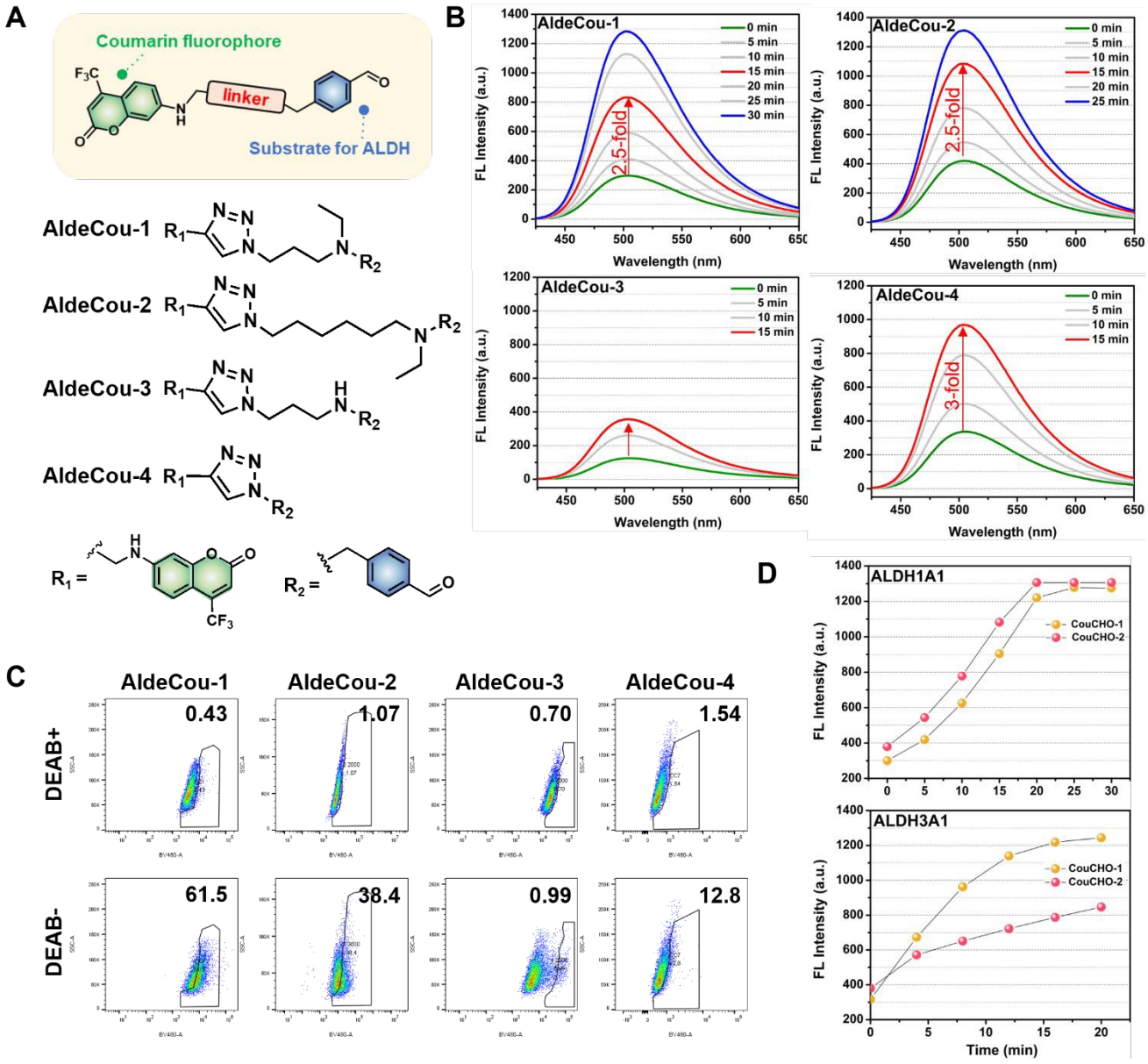

Figure. 1 (A) Chemical structures of coumarin-based ALDH probes **AldeCou-1** to **AldeCou-4** with different triazole-alkyl-amine linkers. (B) Fluorescence spectra of **AldeCou-1** to **AldeCou-4** (10 μM) upon incubation with ALDH1A1 (3.3 μg/mL) and NAD^+ (1 mM) in Tris-buffer (100 mM, pH 7.5) containing 100 mM KCl and 1% DMSO at 37 °C. (C) Flow cytometry analysis of **AldeCou-1** to **AldeCou-4** (2 μM) in A549 cells with or without DEAB (1 mM). (D) Time-dependent fluorescence intensity increase of **AldeCou-1** and **AldeCou-2** after incubating with ALDH1A1 (3.3 μg/mL) with NAD^+ (500 μM) or ALDH3A1 (3.3 μg/mL) with $NADP^+$ (500 μM) (λex/em = 390/490 nm).

View Article Online
DOI: 10.1039/D5TB01253H

Fluorescence turn-on response of AldeCou-1 to ALDH1A1. The absorbance and fluorescence properties of **AldeCou-1** were measured and compared against 7-amino-4-trifluoromethyl coumarin (**Cou**) in pH 7.5 Tris buffer solution (Figure 2A and B). **AldeCou-1** exhibited maximum absorbance (λ_{abs}) and fluorescence (λ_{em}) at 390 and 505 nm, respectively. We also synthesized **AcidCou-1**, the expected enzymatic product of **AldeCou-1**, to test the hypothesis that the respective 4-aminomethyl benzaldehyde fragment of **AcidCou-1** is responsible for the fluorescence turn-on response of the probes. We observed that the fluorescence of **AldeCou-1** is quenched in aqueous Tris-buffer, but not in dichloromethane (Figure S48A). To confirm that this observation in the Tris-buffer is not attributed to aggregation-caused quenching, we implemented fluorescence characterizations of **Cou**, **AldeCou-1**, and **AcidCou-1** in dilute (0.1 μM) and concentrated (1 μM) concentrations in aqueous Tris-buffer and we still observed the fluorescence quenching of **AldeCou-1** in both concentrations (Figure S48 B and C).

Next, we investigated the enzymatic reaction of **AldeCou-1** by incubating it with NAD^+ cofactors and ALDH1A1 enzyme. The fluorescence turn-on mechanism of these probes is expected to be from the oxidation of the 4-aminomethyl benzaldehyde fragment to 4-aminomethyl carboxylate by intracellular ALDH1A1 (Figure S43). The fluorescence intensity of **AldeCou-1** gradually increased over 30 minutes of incubation (Figure 2C), suggesting that the aldehyde functional group in **AldeCou-1** was oxidized into the carboxylate to form **AcidCou-1**. The fluorescence response of the incubated **AldeCou-1** after 30 minutes was compared to synthesized **AcidCou-1**, and the fluorescence profiles and fluorescence intensities of both the enzymatic oxidized product of **AldeCou-1** and synthesized **AcidCou-1** were similar (Figure 2B), further suggesting that the expected **AcidCou-1** be produced from the oxidation of **AldeCou-1**. The oxidation of **AldeCou-1** into **AcidCou-1** was further validated through HPLC analysis, where the incubation of **AldeCou-1** with ALDH1A1 and NAD^+ yielded a new peak after 80 minutes of incubation corresponding to the synthesized **AcidCou-1** peak (Figure 2D). In contrast, incubating **AldeCou-1** with only NAD^+ and without ALDH1A1 showed no fluorescence turn-on response, confirming that the fluorescence turn-on of our probes is due to the oxidative reaction to ALDH1A1 (Figure S49).

View Article Online
DOI: 10.1039/D5TB01253H

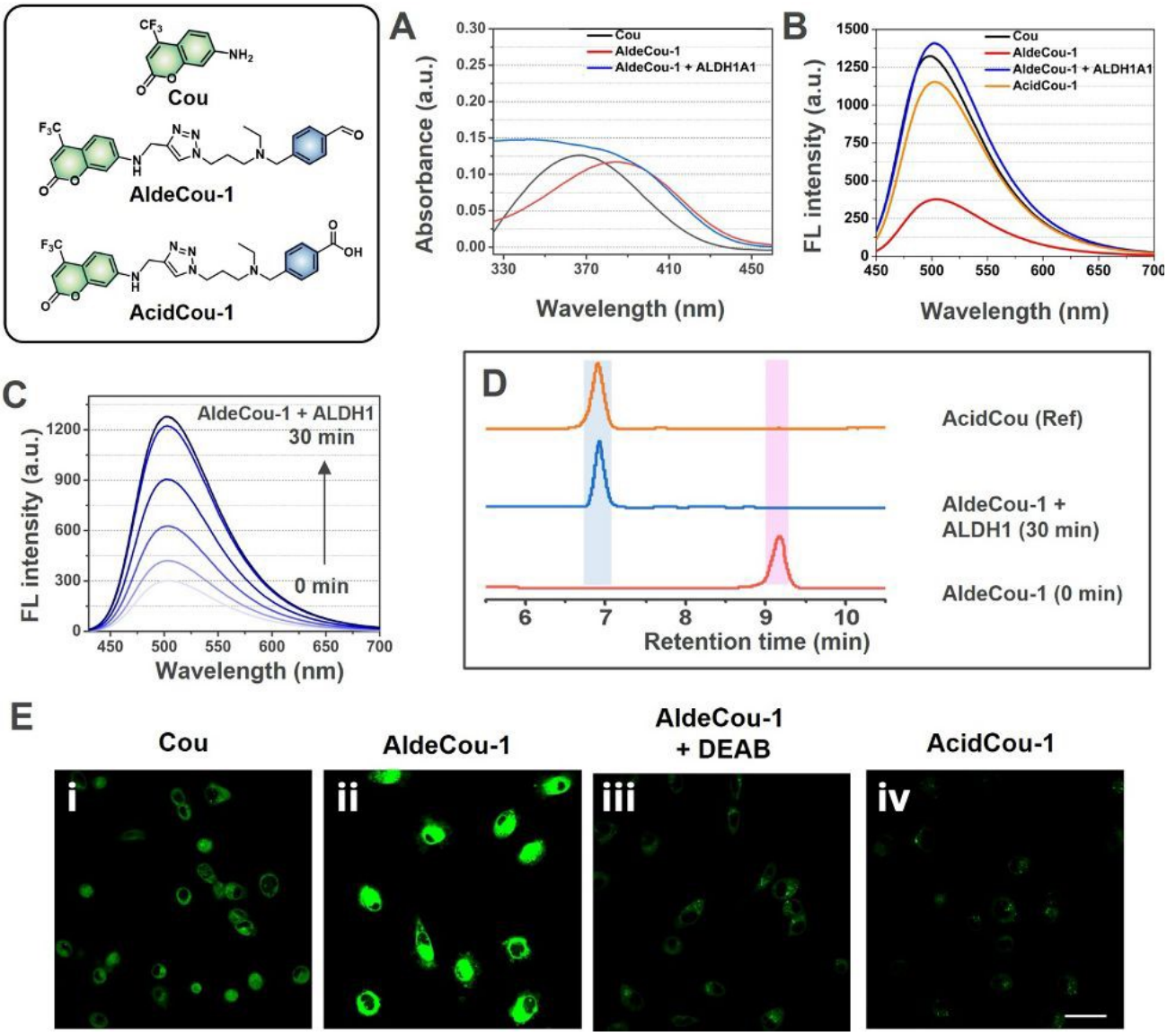

Figure. 2 (A) UV-vis absorption spectra of Cou, **AldeCou-1**, and **AldeCou-1** with ALDH1A1 (10 μM, each) in pH 7.5 Tris buffer with 1% DMSO. Cou: 7-Amino-4-(trifluoromethyl)coumarin. (B) Fluorescence spectra of **Cou** (10 μM), **AldeCou-1** (10 μM), synthesized **AcidCou-1** (10 μM), and **AldeCou-1** incubated with ALDH1A1 (spectra taken from Fig. 2C at the 30th-minute mark). (C) Overlayed fluorescence spectra of **AldeCou-1** (10 μM) with the addition of ALDH1A1 (3.3 μg/mL) and NAD^+ (500 μM), measured for 30 min in pH 7.5 Tris buffer with 1% DMSO at 37 °C. (D) HPLC analysis (absorbance at 365 nm) of synthesized **AcidCou-1** (reference peak), **AldeCou-1** (10 μM) incubated with ALDH1A1 and NAD^+ at 37 °C, and **AldeCou-1** without ALDH1A1 and NAD^+ (E) In vitro live cell fluorescence imaging of MDA-MB-231 cells treated with (i) **Cou** (10 μM), (ii) **AldeCou-1** (10 μM) without DEAB, (iii) **AldeCou-1** (10 μM) with DEAB, and (iv) synthesized **AcidCou-1** (10 μM). Scale bar: 40 μm.

View Article Online
DOI: 10.1039/D5TB01253H

Live cell imaging of AldeCou-1 in MDA-MB-231 cells. The live cell imaging performance of **AldeCou-1** was tested with a standard human breast cancer cell line, MDA-MB-231. We observed a difference between the relative fluorescence intensities of **AldeCou-1** and Cou in aqueous pH 7.5 Tris buffer and in treated MDA-MB-231 cells, where **AldeCou-1** exhibited a much stronger green fluorescence than Cou in MDA-MB-231 cells (Figure 2E i and ii). In contrast, **AldeCou-1** and Cou exhibited similar fluorescence intensities in the aqueous solutions (Figure 2B). The discrepancies in fluorescence intensities of **AldeCou-1** and Cou in solution and in MDA-MB-231 cells can be attributed to their differences in cell membrane permeabilities.[46] Firstly, the oxidation of **AldeCou-1** into **AcidCou-1** by intracellular ALDH present in MDA-MB-231 cells leads to an initial fluorescence turn-on response within MDA-MB-231 cells. To validate this, we separately pretreated MDA-MB-231 cells with DEAB (1 mM), an ALDH inhibitor, before introducing **AldeCou-1** (10 μM). Remarkable fluorescence quenching was observed in the DEAB-pretreated MDA-MB-231 cells (Figure 2E iii), suggesting that the strong fluorescence signal observed in **AldeCou-1** treated MDA-MB-231 cells (Figure 2E ii) was indeed due to oxidation of **AldeCou-1** by ALDH1A1. Secondly, the oxidized product, **AcidCou-1**, contains a benzoic acid fragment that deprotonates into a benzoate at intracellular pH, and thus retaining **AcidCou-1** within the MDA-MB-231 cells. We tested the cell membrane permeability of **AcidCou-1** by treating a solution of MDA-MB-231 cells with synthesized **AcidCou-1** separately, and we observed almost zero fluorescence in these MDA-MB-231 cells after washing (Figure 2E iv). This result indicates no cellular uptake of **AcidCou-1** into the MDA-MB-231 cells, attributed to the low lipophilicity and poor cell membrane permeability of a negatively charged benzoate group. Hence, we inferred that **AcidCou-1** accumulates within MDA-MB-231 cells after sensing ALDH1A1, leading to a strong fluorescence turn-on response within these cells. On the other hand, **Cou**, with no benzoate fragment, has better cell membrane permeability, and its efflux leads to a weaker fluorescence signal observed (Figure 2E i).

View Article Online
DOI: 10.1039/D5TB01253H

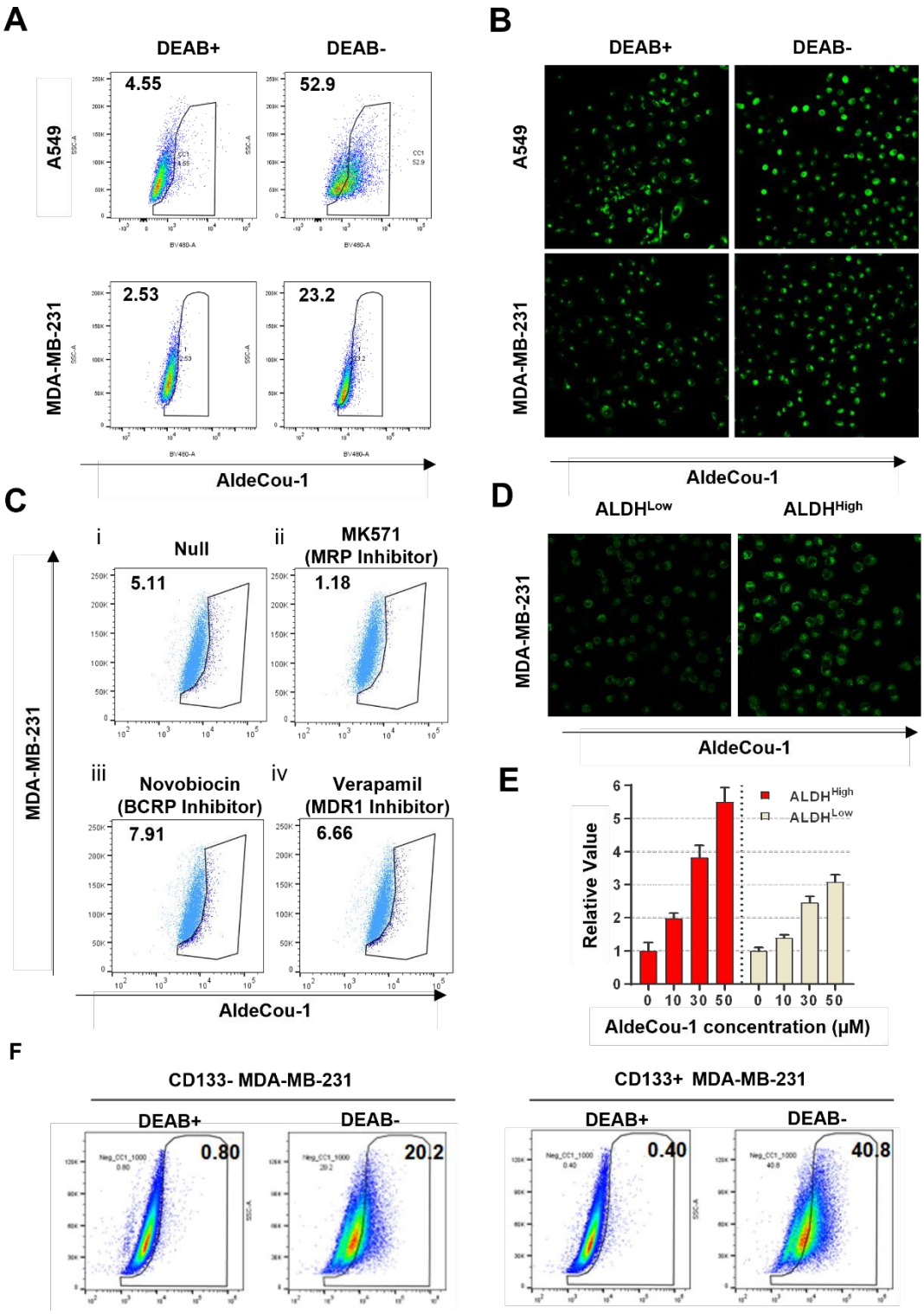

Figure. 3 (A) Flow cytometry analysis of **AldeCou-1** (1 μM) treated A549 and MDA-MB-231 with or without DEAB (1 mM). (B) Confocal live cell imaging of **AldeCou-1** (2 μM) treated A549 and MDA-MB-231 cells. DEAB-treated cells were pretreated with 1 mM DEAB before staining with **AldeCou-1**. (C) Flow cytometry analysis of **AldeCou-1** (10 μM) treated MDA-MB-231 cells without any inhibitors or with MK571 (50 μM), Novobiocin (200 μM), and Verapamil (20 μM) in PBS with 2% FBS. (D) Confocal imaging of $ALDH^{High}$ and

View Article Online
DOI: 10.1039/D5TB01253H

ALDH^{Low} MDA-MB-231 cells treated with **AldeCou-1** (20 μM). Scale bars: 50 μm. (E) Relative fluorescence intensities of ALDH^{High} and ALDH^{Low} MDA-MB-231 cells treated with **AldeCou-1** (0-50 μM) for 2 hours on HBSS (ex/em 390/490 nm). (F) Flow cytometry analysis of **AldeCou-1** probe stained CD133+ and CD133- MDA-MB-231 cells. DEAB was used for negative control. min in pH 7.5 Tris buffer with 1% DMSO at 37 °C.

AldeCou-1 as a potential assay kit for ALDH activity detection. To explore the potential of **AldeCou-1** as a substrate for ALDH activity detection assays, we evaluated its performance against ALDEFLUOR on two ALDH-expressing cell lines, A549 and MDA-MB-231. The first flow cytometry was performed with ALDEFLUOR to establish a baseline of ALDH activities in both A549 and MDA-MB-231 (Figure S50), and another flow cytometry was performed with **AldeCou-1** (Figure 3A) to compare the results against ALDEFLUOR. Both **AldeCou-1** and ALDEFLUOR show similar results of significant CSC population staining (52.9 and 23.2 % in A549 and MDA-MB-231 cell lines with **AldeCou-1**, respectively, and 78.9 and 16.4 % in A549 and MDA-MB-231 cell lines with ALDEFLUOR, respectively). Furthermore, both assays consistently showed higher ALDH activity in A549 compared to MDA-MB-231 cells (Figure 3A and Figure S50), with the live cell imaging and recorded fluorescence intensities of **AldeCou-1** in both A549 and MDA-MD-231 cells, with cells treated with DEAB as a negative control (Figure 3B and Figure S51). Although ALDH1A1 expression levels may vary within a cell population, resulting in greater variability in fluorescence intensities (Figure S51), the average fluorescence intensity in A549 cells is higher than in MDA-MB-231 cells. From this, we conclude that the fluorescence signals observed from **AldeCou-1** assays are attributed to ALDH activity, and **AldeCou-1** can quantitatively visualize ALDH activities in both A549 and MDA-MB-231 cell lines.

As mentioned earlier, ALDEFLUOR assays require the addition of buffers that contain ABC transport inhibitors for accurate quantification of CSCs. Hence, we wanted to investigate the dependency of **AldeCou-1** on ABC transport inhibitors to see if **AldeCou-1** can be employed without additional buffers. We compared assays of **AldeCou-1** without any ABC transport inhibitors to **AldeCou-1** with verapamil, MK-571, and novobiocin (MDR1, MRP1/2, and BCRP inhibitors, respectively). We observed that the population of stained CSCs was consistent between assays with and without ABC transport inhibitors sans MK-57 (5.11% without any inhibitors versus 7.91 and 6.66% in novobiocin and verapamil, respectively). This suggests that including various ABC transporter inhibitors was unnecessary (Figure 3C), improving the conditions needed for an ALDEFLOUR assay.

View Article Online
DOI: 10.1039/D5TB01253H

ALDH activity detection of MDA-MB-231 cells by AldeCou-1. MDA-MB-231 cells were sorted *via* fluorescence-activated cell sorting (FACS) with ALDEFLOUR assay into $ALDH^{High}$ and $ALDH^{Low}$ MDA-MB-231 cells, and were then incubated with **AldeCou-1** for live cell imaging. **AldeCou-1** was able to quantitatively distinguish ALDH activity in these sorted MDA-MB-231 cells, where brighter fluorescence was observed in $ALDH^{High}$ cells compared to $ALDH^{Low}$ cells (Figure 3D and Figure S52). We also compared the difference in fluorescence intensities with varying amounts of **AldeCou-1** (10 – 50 μM) in $ALDH^{High}$ and $ALDH^{Low}$ MDA-MB-231 cells, observing that the fluorescence intensity of **AldeCou-1** is approximately two times stronger in $ALDH^{High}$ than $ALDH^{Low}$ MDA-MB-231 cells, even at low concentrations of **AldeCou-1** used (10 μM) (Figure 3E).

Lastly, we tested if **AldeCou-1** exhibits cell surface protein recognition as an alternative method to detect CSCs. One such surface protein of interest is CD133 (Prominin-1), a marker of CSCs due to its association with proliferation and metastatics.[47, 48] We sorted $CD133^{High}$ and $CD133^{Low}$ MDA-MB-231 cells through MACS sorting, and the sorting was validated using western blot analysis (Figure S53). Then, the sorted MDA-MB-231 cells were stained with **AldeCou-1** and analyzed *via* flow cytometry. We observed that MDA-MB-231 cells with $CD133^{High}$ had significant population staining compared to $CD133^{Low}$ cells (40.8 vs 20.2 %, respectively). This result shows that **AldeCou-1** can quantitatively detect cells with overexpressed CD133 protein (Figure 3F), making **AldeCou-1** a versatile ALDH fluorescent probe for detecting CSCs through both ALDH enzymatic activity and overexpression of CD133 proteins.

View Article Online
DOI: 10.1039/D5TB01253H

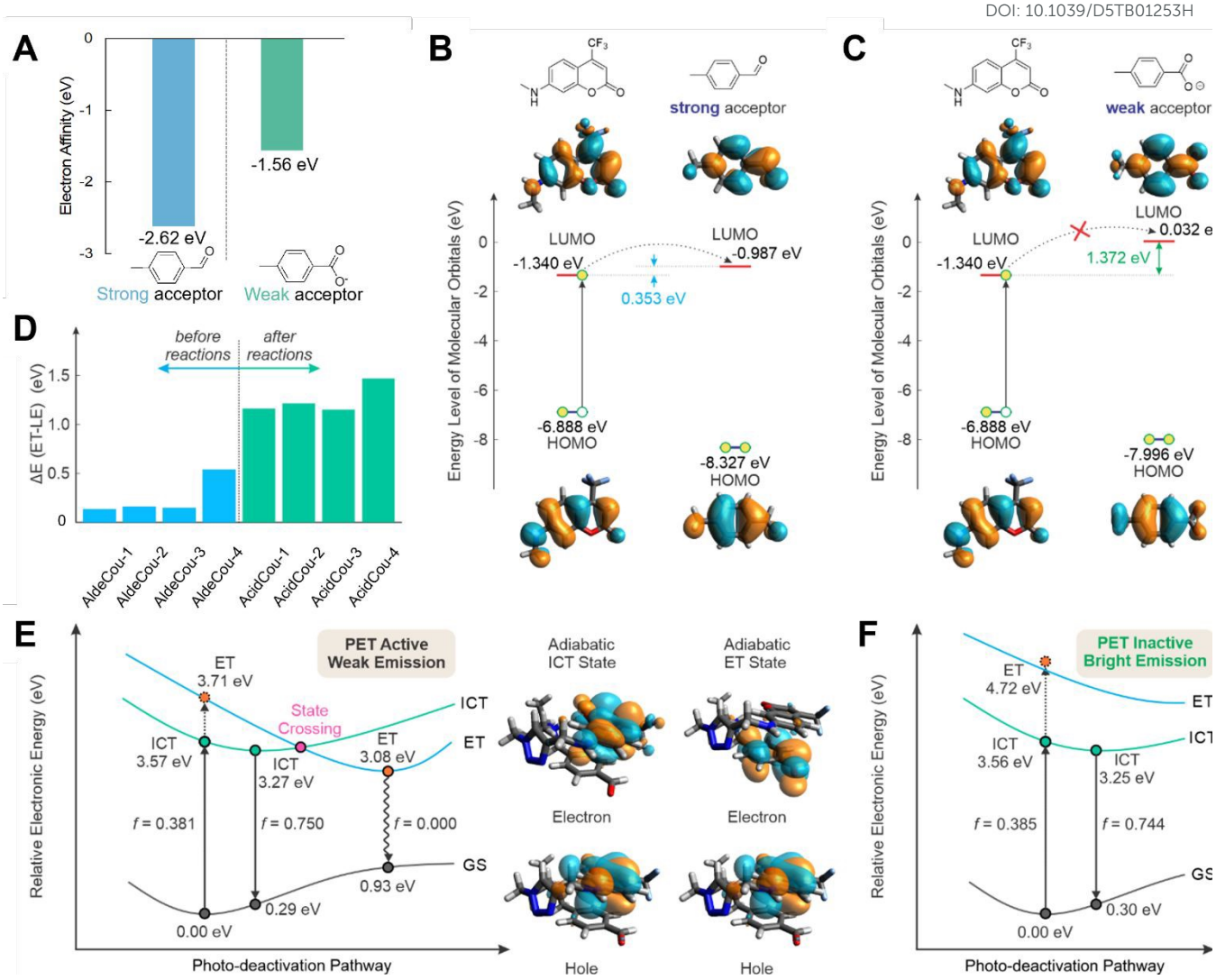

Figure. 4 Theoretical calculations to rationalize the fluorescence turn-on mechanism. (A) Calculated electron affinity of the benzaldehyde and benzoate moieties in water. Comparison of the energy levels of frontier molecular orbitals between coumarin and (B) benzaldehyde, or (C) benzoate in water. (D) Calculated energy gaps between the high-lying electron transfer (ET) and low-lying intramolecular charge transfer (ICT) states in the four probes and their corresponding oxidized products during vertical excitations. (E) Schematic illustration of the state-crossing from an ICT to an ET state and calculated excitation/de-excitation energy (as well as oscillator strength, *f*) of **AldeCou-1** in water; the inset shows the corresponding electron and hole distributions of the adiabatic ICT and ET states. (F) Schematic illustration of the potential energy surface and calculated excitation/de-excitation energy (as well as oscillator strength, *f*) of **AcidCou-**1 in water. The energy levels are not drawn to scale in (E) and (F) for improved clarity.

View Article Online
DOI: 10.1039/D5TB01253H

Computational Studies of AldeCou-1 and elucidation of PET mechanism. Quantum chemical calculations were conducted on **AldeCou-1** to 1) elucidate the fluorescence turn-on mechanism and 2) explain the fluorescence quenching in aqueous environments and bright emission in DCM (Figure S48). Firstly, we calculated the electron affinities (EA) to rationalize the difference in electron-withdrawing strengths of benzaldehyde and benzoate in water. We observe that benzaldehyde exhibits a substantially larger EA (-2.62 eV) compared to benzoate (-1.56 eV) in terms of absolute values, indicating the greater electron-withdrawing capacity of benzaldehyde (Figure 4A). We also analyzed the electronic gap between the frontier molecular orbitals (FMOs) of benzaldehyde, benzoate, and the coumarin moiety (Figures 4B and C, S54 and S55). The pronounced electron-withdrawing nature of benzaldehyde results in a smaller electronic gap (0.353 eV) between the lowest unoccupied molecular orbitals (LUMOs) of coumarin and benzaldehyde, as compared to the more significant electronic gap (1.372 eV) between coumarin and benzoate. The difference in electronic gaps between the LUMOs of coumarin and benzaldehyde or benzoate provides an intuitive basis for predicting that donor-photoinduced electron transfer (d-PET) should be more favorable between coumarin and benzaldehyde than between coumarin and benzoate. Although the calculated LUMO energies of both benzaldehyde and benzoate are higher than that of coumarin—seemingly suggesting that d-PET should not occur—this frontier molecular orbital (FMO) analysis serves only as a preliminary assessment of d-PET feasibility, as it considers only the electronic gap between the donor and acceptor fragments. However, this electronic gap alone fails to account for both exciton binding energy during photoexcitation, and solvent stabilization effects on the electron-transfer (ET) state of the fluorophore *via* strong electrostatic interactions with surrounding polar solvents molecules. Therefore, FMO analysis does not provide an accurate measure of d-PET feasibility alone.[49]

Next, we conducted conformational analysis on the structures of the four probes, given the flexible nature of the alkyl linkers, to arrive at the optimized geometries in the ground state. Interestingly, all probes adopt a folded conformation where the coumarin and benzaldehyde/benzoate fragments exhibit a face-to-face stacking configuration, which is more stable than the extended arrangement (Figure S56, Table S1).[50] We then conducted excited-state calculations on the folded conformations of the four probes to determine the "optical gaps"; given a sufficiently small vertical energy gap (ΔE) between the intramolecular charge transfer (ICT) and ET states upon photo-excitation (Figure 4E, 4F), a state crossing could potentially occur from the ICT to the ET state upon excited state geometry relaxation.[51, 52] For **AldeCou-1**, i.e., before sensing ALDH1A1, vertical ΔE is 0.14 eV (Figure 4E);

View Article Online
DOI: 10.1039/D5TB01253H

while in **AcidCou-1**, i.e., after sensing ALDH1A1, vertical ΔE is significantly widened to 1.16 eV (Figure 4F). This stark difference in ΔE of **AldeCou-1** and **AcidCou-1** suggests that state crossing, and d-PET as a result, could transpire upon relaxation of the excited-state geometry in the former but not in the latter. Performing vertical excited-state calculations on the other probes also yielded a consistent trend of a smaller ΔE in the **AldeCou** series compared to the oxidized **AcidCou** series of the probes (Figure 4D, Table S2).

To validate the occurrence of d-PET in **AldeCou-1**, extensive excited-state calculations to optimize both ICT and ET states revealed a state-crossing (red intersection) between the two states (Figure 4E). Calculations further revealed that the dark ET state (3.08 eV, with nearly zero oscillator strength, *f*) is more stable than the bright ICT state (3.27 eV, $f = 0.750$) by 0.19 eV. This result substantiates the activation of d-PET, effectively quenching the fluorescence of **AldeCou-1**. However, as the driving force for entering the dark ET state is only moderate (0.19 eV), weak emission can still occur through de-excitation from the bright ICT state, which explains two observations of (1) considerable initial background emission of **AldeCou-1** without the addition of ALDH1A1 (Figure 1B) and (2) the modest 2.5-fold increase in fluorescence intensities of **AldeCou-1** upon sensing ALDH1A1 (Figure 1B). Conversely, state crossing and d-PET become unfeasible in **AcidCou-1** due to the large ΔE (Figure 4F). Consequently, a fluorescence turn-on response in the oxidized **AcidCou** product of the probes is observed (Figures S57 – S60), facilitating the monitoring of ALDH1A1 activities. Our computational findings align perfectly with experimental observations, affirming that the modulation of d-PET enables the fluorescence turn-on of the **AldeCou** probes upon reaction with ALDH1A1.

Finally, to address the fluorescence quenching in aqueous medium and the lack thereof in DCM, it is worth noting that d-PET exhibits strong polarity dependence.[49] The d-PET-induced excited ET state has a high polarity due to complete charge separation. In polar solvents (such as water), this ET state is stabilized through strong dipole-dipole interactions with solvent molecules. Conversely, these stabilizing interactions are absent in low-polarity solvents, such as DCM, making the ET state unstable. In other words, d-PET is inactive in non-polar solvents. This polarity dependence explains why fluorescence modulation of our probes is only observable in water but not in DCM.

Conclusion

View Article Online
DOI: 10.1039/D5TB01253H

Four novel ALDH probes were synthesized following a coumarin, 1,2,3-triazole-alkyl-amine linker, and a 4-methylbenzaldehyde fragment, with λ_{abs} ranging from 380 to 395 nm and showed a common maximum emission of λ_{em} at 505 nm. They also exhibited a strong selectivity towards ALDH1A1 over other common physiological analytes. **AldeCou-1** showed the highest percentage of CSC staining in A549 cells with a propensity to detect both ALDH1A1 and ALDH3A1 enzymes; live cell imaging of MDA-MB-231 cells treated with **AldeCou-1** revealed fluorescence turn-on in response to ALDH activity in these CSCs. Flow cytometry analysis suggests the employability of **AldeCou-1** in ALDH activity detection assays. **AldeCou-1** displayed similar quantitative detection capabilities to ALDEFLUOR, distinguishing MDA-MB-231 from A549 cell lines based on CSC staining populations, and identifying $ALDH^{High}$ and $ALDH^{Low}$ cells based on varying fluorescence intensities. **AldeCou-1** can also detect CD133, a surface protein present in CSCs, showcasing the versatility of **AldeCou-1** to mark CSCs *via* both ALDH enzymatic activity and overexpression of CD133 proteins. More importantly, **AldeCou-1** showed little dependency on ABC transporter inhibitors for accurate quantifications of CSCs, removing the need for additional buffers for ALDH assays, a stark improvement to ALDH assay conditions. Computational findings elucidated the working mechanism of our probes, where we discovered that solvent/polarity dependency and substrate-induced PET-on/off were responsible for the fluorescence turn-on response of our probes with ALDH. Overall, the promising experimental and computational findings from this study can provide crucial insights into the design of next-generation ALDH probes, where multi-detection methods of CSCs and simplifying conditions for ALDH activity assays are made possible.

Associated Content

Supporting Information

The data supporting this article have been included as part of the ESI.†

Author Information

Corresponding Authors

*E-mail: jongskim@korea.ac.kr; xiaogang_liu@sutd.edu.sg.

Acknowledgments

View Article Online
DOI: 10.1039/D5TB01253H

This work was supported by the National Research Foundation of Korea (NRF) funded by the Korea Ministry of Science and ICT (MSIT) (CRI project No. 2018R1A3B1052702, J.S.K. and RS-2024-00412235 J.H.K.). The authors would like to acknowledge funding support from the Ministry of Education, Singapore (MOE-T2EP10222-0001), Singapore University of Technology and Design (SUTD) Kickstarter Initiative (grant number: SKI 2021_03_10). The authors are also grateful for the computing service of SUTD and the National Supercomputing Centre (Singapore).

Notes

The authors declare no competing financial interest.

References

1. H. Clevers, *Nat. Med.*, 2011, **17**, 313-319.
2. T. Reya, S. J. Morrison, M. F. Clarke and I. L. Weissman, *Nature*, 2001, **414**, 105-111.
3. A. Turdo, V. Veschi, M. Gaggianesi, A. Chinnici, P. Bianca, M. Todaro and G. Stassi, *Front. Cell Dev. Biol.*, 2019, **7**, 16.
4. H. Clevers, *Nat. Med.*, 2011, **17**, 313.
5. T. Reya, S. J. Morrison, M. F. Clarke and I. L. Weissman, N*ature*, 2001, **414**, 105.
6. A. Turdo, V. Veschi, M. Gaggianesi, A. Chinnici, P. Bianca, M. Todaro and G. Stassi, *Front. Cell Dev. Biol.*, 2019, **7**, 1.
7. A. Z. Ayob and T. S. Ramasamy, *J. Biomed. Sci.*, 2018, **25**, 20.
8. Y. Yang, X. Li, T. Wang, Q. Guo, T. Xi and L. Zheng, *J. Hematol. Oncol.*, 2020, **13**, 60.
9. S. Liu, Y. Cong, D. Wang, Y. Sun, L. Deng, Y. Liu, R. Martin-Trevino, L. Shang, S. P. McDermott, M. D. Landis, S. Hong, A. Adams, R. D'Angelo, C. Ginestier, E. Charafe-Jauffret, S. G. Clouthier, D. Birnbaum, S. T. Wong, M. Zhan, J. C. Chang and M. S. Wicha, *Stem Cell Rep.*, 2014, **2**, 78-91.
10. F. Meng and G. Wu, *Cancer Metastasis Rev.*, 2012, **31**, 455-467.
11. J. Han, M. Won, J. H. Kim, E. Jung, K. Min, P. Jangili and J. S. Kim, *Chem. Soc. Rev.*, 2020, **49**, 7856-7878.
12. R. R. Begicevic and M. Falasca, *Int J Mol Sci*, 2017, **18**.
13. S. Basu, Y. Dong, R. Kumar, C. Jeter and D. G. Tang, *Semin. Cancer Biol.*, 2022, **78**, 90-103.
14. S. A. Marchitti, C. Brocker, D. Stagos and V. Vasiliou, *Expert Opin. Drug Metab. Toxicol.*, 2008, **4**, 697-720.
15. R. Januchowski, K. Wojtowicz and M. Zabel, *Biomed. Pharmacother.*, 2013, **67**, 669-680.
16. N. Ding, Z. Li, Y. Hao and C. Zhang, *Anal. Chem.*, 2022, **94**, 12120-12126.
17. M. Oe, K. Miki, Y. Ueda, Y. Mori, A. Okamoto, Y. Funakoshi, H. Minami and K. Ohe, *ACS Sensors*, 2021, **6**, 3320-3329.
18. S. Li, W. Tang and X. Duan, *New J. Chem.*, 2023, **47**, 545-549.
19. I. Minn, H. Wang, R. C. Mease, Y. Byun, X. Yang, J. Wang, S. D. Leach and M. G. Pomper, *Nat. Commun.*, 2014, **5**, 3662.
20. C. Anorma, J. Hedhli, T. E. Bearrood, N. W. Pino, S. H. Gardner, H. Inaba, P. Zhang, Y. Li, D. Feng and S. E. Dibrell, *ACS Cent. Sci.*, 2018, **4**, 1045.
21. K. Bredael, S. Geurs, D. Clarisse, K. De Bosscher and M. D'hooghe, *J Chem.*, 2022, **2022**, 2164558.
22. A. Yagishita, T. Ueno, K. Tsuchihara and Y. Urano, *Bioconjug. Chem.*, 2021, **32**, 234-238.
23. A. Yagishita, T. Ueno, H. Esumi, H. Saya, K. Kaneko, K. Tsuchihara and Y. Urano, *Bioconjug. Chem.*, 2017, **28**, 302-306.
24. K. Miki, M. Oe, K. Suzuki, K. Miki, H. Mu, Y. Kato, M. Iwatake, H. Yukawa, Y. Baba, Y. Ueda, Y. Mori and K. Ohe, *J. Mater. Chem. B*, 2024, **12**, 6959-6967.
25. C. Anorma, J. Hedhli, T. E. Bearrood, N. W. Pino, S. H. Gardner, H. Inaba, P. Zhang, Y. Li, D. Feng, S. E. Dibrell, K. A. Kilian, L. W. Dobrucki, T. M. Fan and J. Chan, *ACS Cent. Sci.*, 2018, **4**, 1045-1055.
26. T. E. Bearrood, G. Aguirre-Figueroa and J. Chan, *Bioconjug. Chem.*, 2020, **31**, 224-228.

View Article Online
DOI: 10.1039/D5TB01253H

27. R. J. Jones, J. P. Barber, M. S. Vala, M. I. Collector, S. H. Kaufmann, S. M. Ludeman, O. M. Colvin and J. Hilton, *Blood*, 1995, **85**, 2742-2746.
28. J. W. Park, K.-H. Jung, Y. Byun, J. H. Lee, S. H. Moon, Y. S. Cho and K.-H. Lee, *Sci. Rep.*, 2019, **9**, 6462.
29. B. The Huy, D. T. Thangadurai, M. Sharipov, N. Ngoc Nghia, N. Van Cuong and Y.-I. Lee, *Microchem. J.*, 2022, **179**, 107511.
30. R. Wills, R. Shirke, H. Hrncir, J. Talbott, K. Sad, J. Spangle, A. Gracz and M. Raj, *Chem. Sci.*, 2024, **15,** 4763-4769.
31. J. F. Araneda, W. E. Piers, B. Heyne, M. Parvez and R. McDonald, *Angew. Chem. Int. Ed.*, 2011, **50**, 12214-12217.
32. J. H. Kim, P. Verwilst, M. Won, J. Lee, J. L. Sessler, J. Han and J. S. Kim, *J. Am. Chem. Soc.*, 2021, **143**, 14115-14124.
33. A. D. Becke, *J. Chem. Phys.* 1993, **98**, 5648-5652.
34. G. Scalmani, M. J. Frisch, B. Mennucci, J. Tomasi, R. Cammi and V. Barone, *J. Chem. Phys.*, 2006, **124**, 94107.
35. M. J. Frisch, G. W. Trucks, H. B. Schlegel, G. E. Scuseria, M. A. Robb, J. R. Cheeseman, G. Scalmani, V. Barone, G. A. Petersson, H. Nakatsuji, X. Li, M. Caricato, A. V. Marenich, J. Bloino, B. G. Janesko, R. Gomperts, B. Mennucci, H. P. Hratchian, J. V. Ortiz, A. F. Izmaylov, J. L. Sonnenberg, Williams, F. Ding, F. Lipparini, F. Egidi, J. Goings, B. Peng, A. Petrone, T. Henderson, D. Ranasinghe, V. G. Zakrzewski, J. Gao, N. Rega, G. Zheng, W. Liang, M. Hada, M. Ehara, K. Toyota, R. Fukuda, J. Hasegawa, M. Ishida, T. Nakajima, Y. Honda, O. Kitao, H. Nakai, T. Vreven, K. Throssell, J. A. Montgomery Jr., J. E. Peralta, F. Ogliaro, M. J. Bearpark, J. J. Heyd, E. N. Brothers, K. N. Kudin, V. N. Staroverov, T. A. Keith, R. Kobayashi, J. Normand, K. Raghavachari, A. P. Rendell, J. C. Burant, S. S. Iyengar, J. Tomasi, M. Cossi, J. M. Millam, M. Klene, C. Adamo, R. Cammi, J. W. Ochterski, R. L. Martin, K. Morokuma, O. Farkas, J. B. Foresman and D. J. Fox, Gaussian, Inc., Wallingford CT, 2016.
36. J. D. Chai and M. Head-Gordon, *Phys. Chem. Chem. Phys.*, 2008, **10**, 6615-6620.
37. F. Weigend and R. Ahlrichs, *Phys. Chem. Chem. Phys.*, 2005, **7**, 3297-3305.
38. Y. Zhao and D. G. Truhlar, *Theor. Chem. Acc.*, 2008, **120**, 215-241.
39. A. J. Cohen and N. C. Handy, *Mol. Phys.* 2001, **99**, 607-615.
40. G. A. Petersson and M. A. Al-Laham, *J. Chem. Phys.*, 1991, **94**, 6081-6090.
41. A. V. Marenich, C. J. Cramer and D. G. Truhlar, *J. Phys. Chem. B.*, 2009, **113**, 6378-6396.
42. K. V. Mikkelsen, P. Jo/rgensen and H. J. r. A. Jensen, *J. Chem. Phys.*, 1994, **100**, 6597-6607.
43. M. Caricato, B. Mennucci, J. Tomasi, F. Ingrosso, R. Cammi, S. Corni and G. Scalmani, *J. Chem. Phys.*, 2006, **124**, 124520.
44. M. D. Hanwell, D. E. Curtis, D. C. Lonie, T. Vandermeersch, E. Zurek and G. R. Hutchison, *J. Cheminform.* 2012, **4**, 1-17.
45. J. Xia, S. Li, S. Liu and L. Zhang, *MedComm.*, 2023, **4**, e195.
46. J. H. Kim, J. Lee, K.-W. Lee, H. Xiong, M. Li and J. S. Kim, *JACS Au*, 2024, **4**, 3657-3667.
47. F. Brugnoli, S. Grassilli, Y. Al-Qassab, S. Capitani and V. Bertagnolo, *J. Oncol.*, 2019, **2019**, 7512632.
48. C. Joseph, M. Arshad, S. Kurozomi, M. Althobiti, I. M. Miligy, S. Al-Izzi, M. S. Toss, F. Q. Goh, S. J. Johnston, S. G. Martin, I. O. Ellis, N. P. Mongan, A. R. Green and E. A. Rakha, *Breast Cancer Res. Treat.*, 2019, **174**, 387-399.
49. W. Chi, J. Chen, W. Liu, C. Wang, Q. Qi, Q. Qiao, T. M. Tan, K. Xiong, X. Liu, K. Kang, Y.-T. Chang, Z. Xu and X. Liu, *J. Am. Chem. Soc.*, 2020, **142**, 6777-6785.
50. S. Huang, S. A. A. Abedi, Z. Li, R. Huang, X. Yan, M. Izadyar, Q. Qiao, Y. Fang, Z. Xu and X. Liu, *CCS Chem.*, 2024, **6**, 2804-2813.
51. K. A. Zachariasse, T. v. d. Haar, A. Hebecker, U. Leinhos and W. Kuhnle, *Pure Appl. Chem.*, 1993, **65**, 1745-1750.
52. R.-X. He and X.-Y. Li, *Chem. Phys.*, 2007, **332**, 325-335.

View Article Online
DOI: 10.1039/D5TB01253H

Data availability statement

The data supporting this article have been included as part of the ESI.†